Three-Phase Photovoltaic System With Three-Level Boosting MPPT Control

Jung-Min Kwon, *Student Member, IEEE*, Bong-Hwan Kwon, *Member, IEEE*, and Kwang-Hee Nam, *Member, IEEE*

***Abstract*—This paper proposes a three-phase photovoltaic (PV) system with three-level boosting maximum power point tracking (MPPT) control. A simple MPPT control using a power hysteresis tracks the maximum power point (MPP), giving direct duty control for the three-level boost converter. The three-level boost converter reduces the reverse recovery losses of the diodes. Also, a weighted-error proportional and integral (PI) controller is suggested to control the dc link voltage faster. All algorithms and controllers were implemented on a single-chip microprocessor. Experimental results obtained on a 10-kW prototype show high performance, such as an MPPT efficiency (MPPT effectiveness) of 99.6%, a near-unity power factor, and a power conversion efficiency of 96.2%.**

***Index Terms*—Maximum power point tracking (MPPT), photovoltaic (PV) system, three-level boost converter.**

I. Introduction

ENVIRONMENTAL concerns about global warming, fossil fuel exhaustion, and the need to reduce carbon dioxide emissions provide the stimulus to seek renewable energy sources. Specifically, solar energy has the advantages of no pollution, low maintenance cost, no installation area limitation, and no noise due to the absence of the moving parts. However, high initial capital cost and low energy conversion efficiency have deterred its popularity. Therefore, it is important to reduce the installation cost and to increase the energy conversion efficiency of photovaltaic (PV) arrays and the power conversion efficiency of PV systems.

PV arrays are known to be nonlinear, and there exists one operating point where the PV array generates maximum power. In order to achieve maximum utilization efficiency of the PV array, the MPPT control technique, which extracts the maximum possible power from the PV array, is essential. Various MPPT control methods have been proposed, such as the lookup table method [1], [2], incremental conductance (IC) method [3]–[6], and perturb-and-observe (P&O) method [6]–[9]. The lookup table method requires prior examination of the PV array characteristics. However, PV array characteristics depend on many complex factors, such as temperature, aging, and the possible breakdown of individual cells. Therefore, it is difficult to record and store all possible system conditions [1], [2]. In contrast, the IC method and P&O method have an advantage of not requiring solar panel characteristics. The IC method uses the PV array's incremental conductance dI/dV. At the MPP, it utilizes an expression derived from the condition $dP/dV = 0$. This method provides good performance under rapidly changing conditions [3]–[5]. The P&O method perturbs the operating voltage of the PV array in order to find the direction change for maximizing power. If power increases, then the operating voltage is further perturbed in the same direction, whereas if it decreases, then the direction of operating voltage perturbation is reversed [6]–[9]. This paper suggests a simple MPPT method for the three-level boost converter. This MPPT control uses power hysteresis to track the MPP, giving direct duty control.

As a conventional PV system, a single-stage inverter with transformer is widely utilized. Its circuit has advantages in that much more utility grid-tie voltage options can be selected by selecting different turns ratios of the isolation transformer. However, the transformer lowers the overall power efficiency and increases the cost and the size [10]. Recently, two-stage PV systems have been proposed without the bulky 50/60 Hz step-up transformer [11]–[15]. These transformerless PV systems have the advantages of small size and reduced cost.

This paper proposes a three-phase PV system composed of a three-level boost converter and a three-phase inverter as shown in Fig. 1. The three-level boost converter reduces the switching losses and the reverse recovery losses. The interleaving technique is utilized for the three-level boost converter to reduce the input filter size by input current ripple cancellation. Also, EMI is lower since the PWM actions are happening between half output voltages. A weighted-error PI controller is suggested for fast dc link voltage control. All control functions are implemented fully in software with a single-chip microprocessor. Thus, the three-phase PV system is realized with minimal hardware and at low cost. Experimental results obtained on a 10-kW prototype show high performance, such as wide range of the PV voltage, high MPPT efficiency (99.6%), high power conversion efficiency (96.2%), a near-unity power factor, and low current THD (2.0%).

II. System Control and Analysis

The proposed PV system is composed of the three-level boost converter and the three-phase inverter. The three-level boost converter performs MPPT control and also gives step-up function of the PV voltage. The three-phase inverter regulates the dc link voltage and generates the ac power. Thus, the three-phase inverter performs a step-down function. The power converter with step up/down function allows a wide range of PV voltages. The three-level boost converter has several advantages in high voltage applications such as reduced switching losses and reduced reverse recovery losses of the diode [16]–[18]. The high

Manuscript received January 02, 2008; revised April 23, 2008. Current version published November 21, 2008. Recommended by Associate Editor R. Teodorescu.

The authors are with the Department of Electronic and Electrical Engineering, Pohang University of Science and Technology, Pohang 790-784, Kyungbuk, South Korea (e-mail: jmkwon@postech.ac.kr; bhkwon@postech.ac.kr; kwnam@postech.ac.kr).

Color versions of one or more of the figures in this paper are available online at http://ieeexplore.ieee.org.

Digital Object Identifier 10.1109/TPEL.2008.2001906

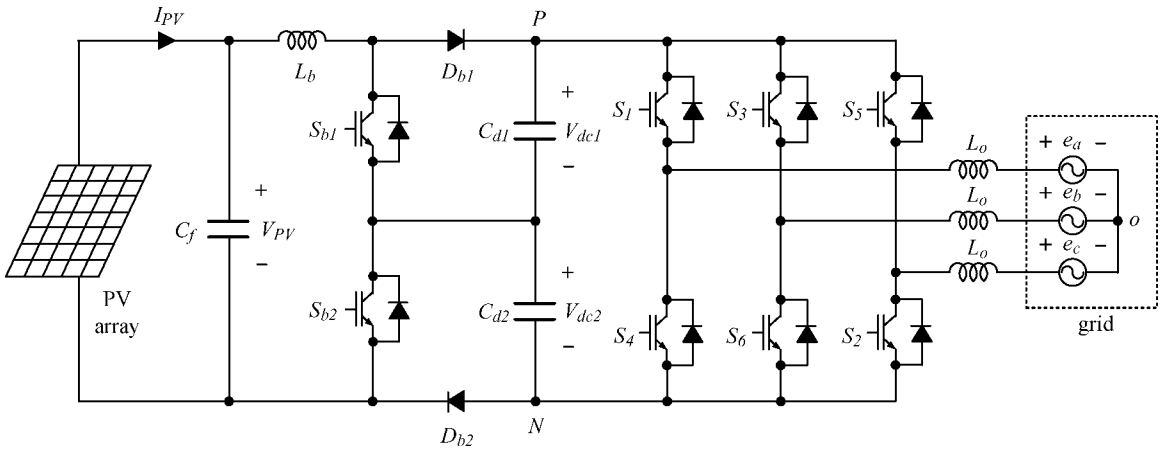

Fig. 1. Proposed three-phase PV system.

voltage rated IGBT used in the conventional boost converter has a larger on-drop voltage than the low voltage rated IGBT. However, the IGBT used in the three-level boost converter has half the rating of that used in the conventional boost converter. Assuming the same output capacitance for devices with different voltage ratings, the capacitive turn-on loss of the three-level boost converter is reduced eight times. The reverse recovery losses of the diode are also reduced, since the reverse voltage is half of the output dc link voltage, and the diodes with half voltage rating are faster.

A. Maximum Power Point Tracking

The P&O method has an advantage of not requiring solar panel characteristics as inputs and being easy to implement. This paper suggests a simple P&O method for the three-level boost converter. The MPPT process and its flowchart are shown in Figs. 2 and 3, respectively. The $flag$ denotes the duty direction for MPPT. The PV voltage is decreased when the $flag$ is 0 and increased when the $flag$ is 1. Therefore, in Fig. 2, the $flag$s of paths ①, ②, and ③ are 0, and the $flag$s of paths ④ and ⑤ are 1. The starting point is the open circuit voltage point. At startup of the MPPT control, the $flag$, P_h, $P_{\rm past}$, and $P_{\rm reverse}$ are initialized as follows:

$$\begin{aligned} flag &= 0 \\ P_{\rm past} &= P_h \\ P_{\rm reverse} &= 0. \end{aligned} \tag{1}$$

The current PV power $P_{\rm PV}$ is calculated by the PV voltage $V_{\rm PV,avg}$ and the PV current $I_{\rm PV,avg}$, which are averaged during the MPPT control period. After the startup of the MPPT control, the operating point moves to MPP through the path ① and ②. After the operating point reaches the MPP, the operating point varies between point B and point D. Point B and point D are determined by the comparative power $P_{\rm reverse}$ for the MPPT direction. The comparative power $P_{\rm reverse}$ has a hysteresis characteristic as follows:

$$P_{\rm reverse} = P_{\rm past} - P_h \tag{2}$$

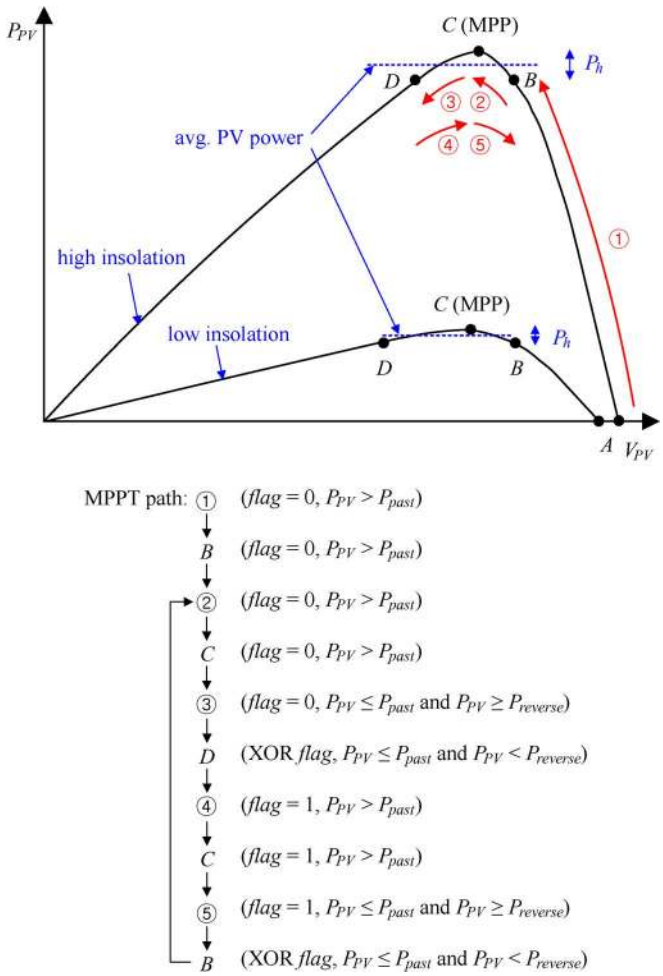

Fig. 2. MPPT process.

where $P_{\rm past}$ is the PV power updated at the previous cycle and P_h is the power hysteresis for perturbing the power variation. Finally, the duty ratio direction of the three-level boost converter is directly determined by the $flag$. The duty ratio is increased when the $flag$ is 0 and decreased when the $flag$ is 1.

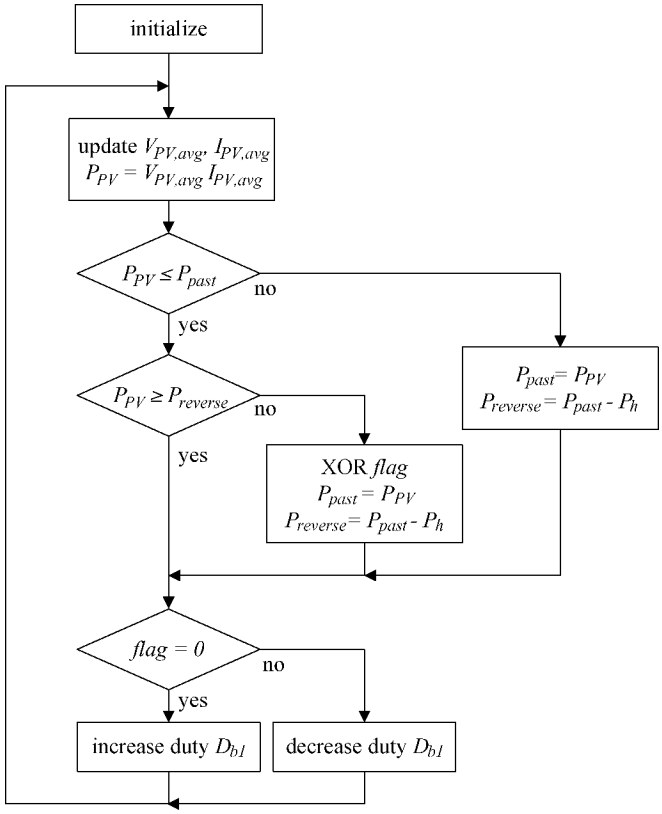

Fig. 3. Flowchart of the MPPT control.

B. Three-Level Boost Converter and DC Link Voltage Balancing Control

When the duty ratio is less than 0.5, the waveforms of the three-level boost converter are shown in Fig. 4(a). Prior to t_0, switches S_{b1} and S_{b2} are turned off. At t_0, which is the beginning of a switching cycle, the switch S_{b1} is turned on and the current flows through L_b, S_{b1}, C_{d2}, and D_{b2}. The PV current I_{PV} increases as follows:

$$I_{\rm PV}(t) = I_{\rm PV}(t_0) + \frac{V_{\rm PV} - V_{\rm dc}/2}{L_b}(t - t_0) \tag{3}$$

where

$$V_{\rm dc} = V_{\rm dc1} + V_{\rm dc2}. \tag{4}$$

At t_1, the switch S_{b1} is turned off and both switches are not conducting. The current flows through L_b, D_{b1}, C_{d1}, C_{d2}, and D_{b2}, and the PV current I_{PV} decreases as follows:

$$I_{\rm PV}(t) = I_{\rm PV}(t_1) - \frac{V_{\rm dc} - V_{\rm PV}}{L_b}(t - t_1). \tag{5}$$

At t_2, the switch S_{b2} is turned on and the current flows through L_b, D_{b1}, C_{d1}, and S_{b2}. The PV current $I_{\rm PV}$ increases like as (3). At t_3, the switch S_{b2} is turned off and both switches are not conducting. The current flows through L_b, D_{b1}, C_{d1}, C_{d2}, and D_{b2}. The PV current I_{PV} decreases, as in (5).

When the duty ratio is grater than 0.5, the waveforms of the three-level boost converter are shown in Fig. 4(b). Prior to t_0, the switch S_{b1} is turned off and the switch S_{b2} is turned on. At t_0, the switch S_{b1} is turned on and both switches are conducting. The PV current $I_{\rm PV}$ increases like a conventional boost converter

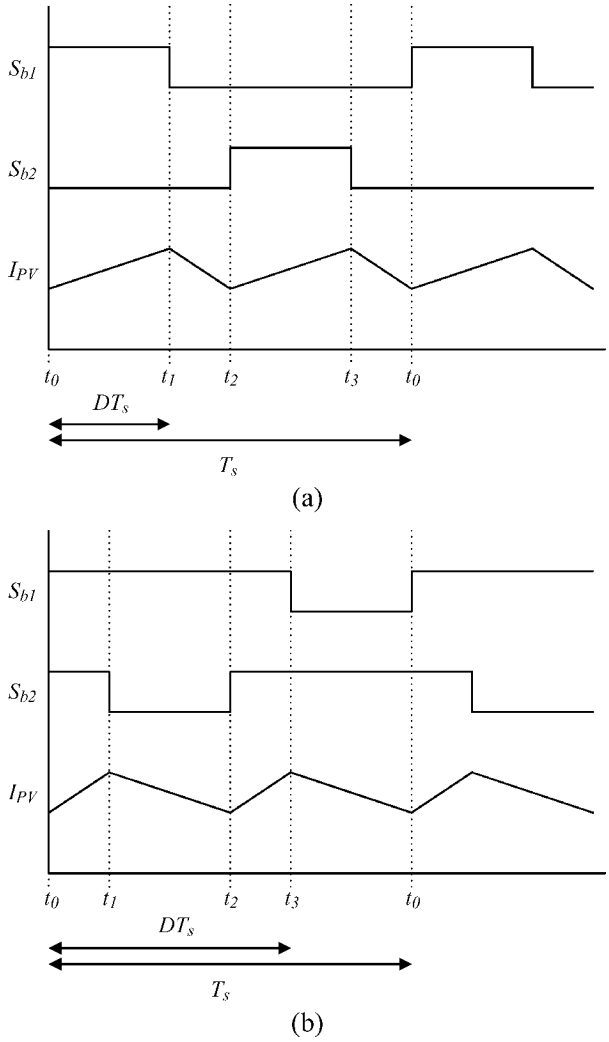

Fig. 4. Theoretical waveforms of the three-level boost converter. (a) $D_{b1} \le 0.5$. (b) $D_{b1} > 0.5$.

$$I_{\rm PV}(t) = I_{\rm PV}(t_0) + \frac{V_{\rm PV}}{L_b}(t - t_0). \tag{6}$$

At t_1, the switch S_{b2} is turned off and the current flows through L_b, S_{b1}, C_{d2}, and D_{b2}. The PV current $I_{\rm PV}$ decreases as follows:

$$I_{\rm PV}(t) = I_{\rm PV}(t_1) - \frac{V_{\rm dc}/2 - V_{\rm PV}}{L_b}(t - t_1). \tag{7}$$

At t_2, the switch S_{b2} is turned on and both switches are conducting. The PV current $I_{\rm PV}$ increases again, as in (6). At t_3, the switch S_{b1} is turned off and the current flows through L_b, D_{b1}, C_{d1}, and S_{b2}. The PV current $I_{\rm PV}$ decreases as in (7).

Since the capacitors C_{d1} and C_{d2} are alternatively charged, their voltages $V_{\rm dc1}$ and $V_{\rm dc2}$ are theoretically balanced. In reality, they are not since the parameters of the components are not exactly balanced. To ensure equal voltages of the two capacitors $V_{\rm dc1}$ and $V_{\rm dc2}$, a voltage balancing controller is essential. Fig. 5 shows the controller of the three-level boost converter

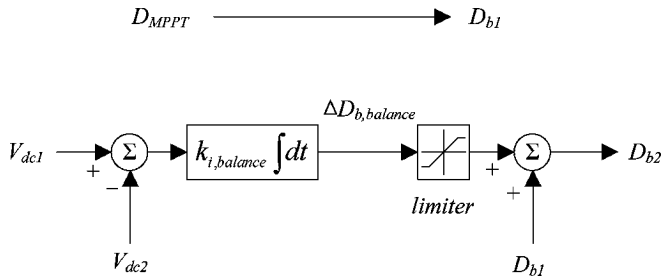

Fig. 5. DC link voltage balancing controller.

that ensures equal balancing of the dc link voltages $V_{\rm dc1}$ and $V_{\rm dc2}$. The duty ratio of the boost switch S_{b1} is determined by the MPPT control and the duty ratio of the boost switch S_{b2} is determined by adding an additional duty for the dc link voltage balance $\Delta D_{b,\rm balance}$. The additional duty for current balance $\Delta D_{b,\rm balance}$ is

$$\Delta D_{b,\rm balance} = k_{i,\rm balance}\int (V_{\rm dc1} - V_{\rm dc2})dt \tag{8}$$

where $k_{i,\rm balance}$ is the integral control gain of the dc link voltage balancing controller.

The total dc link voltage $V_{\rm dc}(= V_{\rm dc1} + V_{\rm dc2})$ is regulated by the inverter. As the dc link voltage $V_{\rm dc}$ is increased, the inverter increases the output power. On the other hand, as the dc link voltage $V_{\rm dc}$ is decreased, the inverter decreases the output power.

C. Fast DC Link Voltage Control

In Fig. 1, e_a, e_b, and e_c are the grid voltages and v_{ao}, v_{bo}, and v_{co} are the output leg voltages. i_a, i_b, and i_c are the output currents. The voltage equations in the stationary $a-b-c$ frame are

$$\begin{aligned} e_a &= E\cos\omega t = -L_o\frac{di_a}{dt} + v_{ao} \\ e_b &= E\cos\left(\omega t - \frac{2}{3}\pi\right) = -L_o\frac{di_b}{dt} + v_{bo} \\ e_c &= E\cos\left(\omega t - \frac{4}{3}\pi\right) = -L_o\frac{di_c}{dt} + v_{co} \end{aligned} \tag{9}$$

where E and ω are the maximum phase voltage and angular frequency of the grid, respectively. The voltage equations in the stationary frame are given by

$$\begin{bmatrix} e_x \\ e_y \end{bmatrix} = \frac{2}{3}\begin{bmatrix} 1 & -\frac{1}{2} & -\frac{1}{2} \\ 0 & \frac{\sqrt{3}}{2} & -\frac{\sqrt{3}}{2} \end{bmatrix}\begin{bmatrix} e_a \\ e_b \\ e_c \end{bmatrix} = \begin{bmatrix} -L_o\frac{di_x}{dt} + v_x \\ -L_o\frac{di_y}{dt} + v_y \end{bmatrix}. \tag{10}$$

The voltage equations in the synchronous $d-q$ frame are given by

$$\begin{aligned} \begin{bmatrix} e_d \\ e_q \end{bmatrix} &= \begin{bmatrix} \cos(\omega t) & \sin(\omega t) \\ -\sin(\omega t) & \cos(\omega t) \end{bmatrix}\begin{bmatrix} e_x \\ e_y \end{bmatrix} \\ &= \begin{bmatrix} \cos(\omega t) & \sin(\omega t) \\ -\sin(\omega t) & \cos(\omega t) \end{bmatrix}\left(-L_o\frac{d}{dt}\right) \\ &\quad \cdot \begin{bmatrix} \cos(\omega t) & \sin(\omega t) \\ -\sin(\omega t) & \cos(\omega t) \end{bmatrix}^{-1}\begin{bmatrix} i_d \\ i_q \end{bmatrix} + \begin{bmatrix} v_d \\ v_q \end{bmatrix} \\ &= -L_o\frac{d}{dt}\begin{bmatrix} i_d \\ i_q \end{bmatrix} - \omega L_o\begin{bmatrix} -i_q \\ i_d \end{bmatrix} + \begin{bmatrix} v_d \\ v_q \end{bmatrix} \end{aligned} \tag{11}$$

where e_d and i_d are the d-axis output voltage and current, and e_q and i_q are the q-axis output voltage and current. The grid voltages of dq-axis are $e_d = \rm E$ and $e_q = 0$. For a unity power factor, it is desirable that the q-axis current i_q is zero. Then the q-axis current i_q is controlled with the zero reference current $i_q^* = 0$. The active power P supplied to the grid is

$$P = \frac{3}{2}(e_d i_d + e_q i_q) = \frac{3}{2}e_d i_d = \frac{3}{2}Ei_d. \tag{12}$$

Since the active power P is directly proportional to the d-axis current i_d, the d-axis reference current i_d^* is generated from the PI voltage controller for the dc link voltage regulation. The conventional PI voltage controller is

$$i_d^* = k_p e + k_i\int e dt \tag{13}$$

$$e = V_{\rm dc}^* - V_{\rm dc} \tag{14}$$

where $V_{\rm dc}^*$ and $V_{\rm dc}$ are the reference dc link voltage and the dc link voltage, k_p and k_i are the proportional and integral control gains of the PI voltage controller, and e is the error voltage between $V_{\rm dc}^*$ and $V_{\rm dc}$. The regulated dc link voltage is an important factor for achieving high performance. However, the conventional PI voltage controller controls the dc link voltage slowly and the dc link voltage variation exists. To reduce the dc link voltage variation, a weighted-error PI voltage controller is suggested. The suggested controller is

$$i_d^* = k_p e_w + k_i\int e_w dt \tag{15}$$

$$e_w = (V_{\rm dc}^* - V_{\rm dc}) \times \left(1 + \frac{|V_{\rm dc}^* - V_{\rm dc}|}{\alpha}\right) \tag{16}$$

where e_w is the weighted-error between $V_{\rm dc}^*$ and $V_{\rm dc}$, and α is the weighting scale factor. Compared to the error term of the conventional PI voltage controller in (14), the $|V_{\rm dc}^* - V_{\rm dc}|/\alpha$ term is included. Fig. 6 shows the difference of the error term of the conventional PI controller (14) and the error term of the suggested weighted-error PI controller (16). The horizontal axis represents the difference of $V_{\rm dc}^*$ and $V_{\rm dc}$, and the vertical axis represents the weighted error e_w. Due to the term of $|V_{\rm dc}^* - V_{\rm dc}|/\alpha$ in error term of the suggested controller, a large error between $V_{\rm dc}^*$ and $V_{\rm dc}$ increases the weighted-error e_w more than the error voltage of the conventional PI controller e. Therefore, if the voltage error is large, then the dc link voltage is controlled rapidly as the PI controller has a large gain. In contrast, if the voltage error is small, the suggested controller gives almost the same characteristic as the conventional PI controller. Since the stability problem based on the small-signal analysis is handled with almost zero voltage error, the stability of the proposed weighted-error-based PI controller is almost the same as the conventional PI controller.

D. Current Controller for Unity Power Factor

The voltage equations (9) are transformed from the stationary $a-b-c$ frame to the synchronous $d-q$ frame as follows:

$$\begin{aligned} E &= -L_o\frac{di_d}{dt} + \omega L_o i_q + v_d \\ 0 &= -L_o\frac{di_q}{dt} - \omega L_o i_d + v_q. \end{aligned} \tag{17}$$

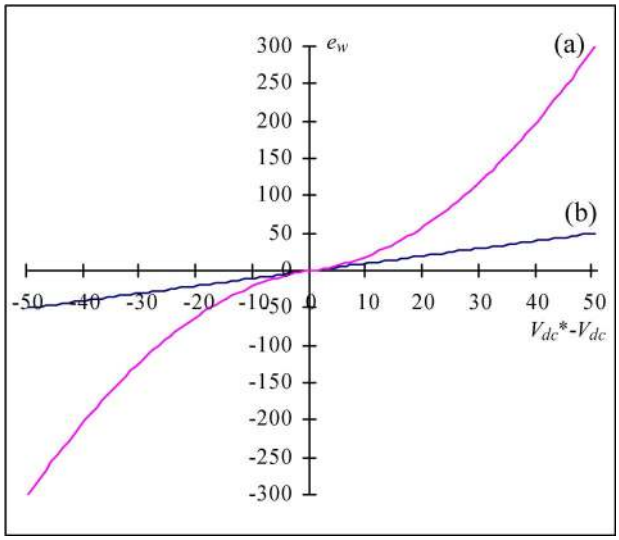

Fig. 6. Difference of (a) the error term of the suggested weighted-error PI controller ($\alpha = 10$) and (b) the error term of the conventional PI controller.

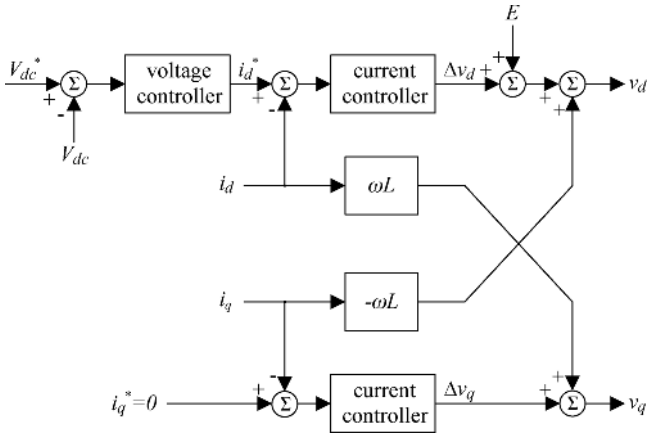

Fig. 7. Decoupled control diagram for three-phase inverter.

To make the input currents track the reference currents, the PI current controllers can be utilized. However, the PI current controllers do not work well as rapid tracking controllers for the coupled system in (17). To avoid this problem, the following decoupling control is effective:

$$\begin{aligned} v_d &= E - \omega L_o i_q + \Delta v_d \\ v_q &= \omega L_o i_d + \Delta v_q. \end{aligned} \tag{18}$$

With the addition of the overall current controller (18) to the inverter (17), which is originally a coupled dynamic system, the input-output relations of the inverter become first-order decoupled linear dynamic systems with easy controllability as follows:

$$\begin{aligned} 0 &= -L_o \frac{di_d}{dt} + \Delta v_d \\ 0 &= -L_o \frac{di_q}{dt} + \Delta v_q. \end{aligned} \tag{19}$$

The output signals Δv_d and Δv_q of the current controllers generate transient additional voltages required to maintain the sinusoidal input currents

$$\begin{aligned} \Delta v_d &= k_{pd}\left(i_d^* - i_d\right) + k_{id}\int \left(i_d^* - i_d\right) dt \\ \Delta v_q &= k_{pq}\left(i_q^* - i_q\right) + k_{iq}\int \left(i_q^* - i_q\right) dt. \end{aligned} \tag{20}$$

k_{pd} and k_{pq} are proportional control gains and k_{id} and k_{iq} are integral control gains. Thus, the overall current controller in the synchronous reference frame relaxes the burden of the PI current controllers and improves the input current waveform. Fig. 7 shows the decoupled control diagram for the inverter system.

The PWM pulses of the three-phase inverter are generated by the space-vector modulation (SVM) technique. The SVM technique is a popular PWM method for the three-phase inverter with isolated neutral load because of two excellent features: Its maximum output voltage is 15.5% greater and the number of switching is about 33% less at the same carrier frequency than the ones obtained by the sinusoidal pulse-width modulation method. An effective software implementation of the SVM for current control on the rotating frame [19] is adopted.

III. Experimental Results

The hardware circuit of the three-phase PV system in Fig. 1 is implemented. It is divided into two parts: the microprocessor-based control circuit and the power circuit. In the microprocessor-based control system, software flexibility facilitates the development and updating of control algorithms and allows modern control theory to be adopted for higher performance. Moreover, a single-chip microprocessor can implement the controller at a lower cost and a smaller size than a general-purpose microprocessor with accompanying external circuits. The overall control diagram of the PV system, as shown in Fig. 8, is implemented fully in software using a single-chip microprocessor, Microchip dsPIC30F6015. Voltage and current signals are measured by using the 10-bit analog-to-digital (A/D) converter in the microprocessor. The implementation of the voltage and current controllers is performed every sample period of 100 μs. Also, the MPPT controller is performed every 100-ms period.

The selected PV array parameters for the experimental results are presented in Table I. The three-phase PV system was tested over the 380-V line-to-line output voltage, and the switching frequencies of the three-level boost converter and the inverter were 10 kHz. The major components and parameters of the hardware circuit used for experiments are presented in Table II. A photograph of the experimental setup of the three-phase PV system is shown in Fig. 9.

The perturbing power variation for searching the MPP is dependent on the power hysteresis P_h. If the power hysteresis P_h is too small, the MPPT control becomes very sensitive and can be easily disturbed by the measurement uncertainty even though averaged sensing data is used. For proper MPPT operation, the power hysteresis P_h should be greater than the maximum measurement error. However, a large power hysteresis P_h decreases the MPPT efficiency at a low insolation. To overcome this problem, a variable power hysteresis P_h relative to the PV power (insolation) is used. Thus, the perturbing power variation

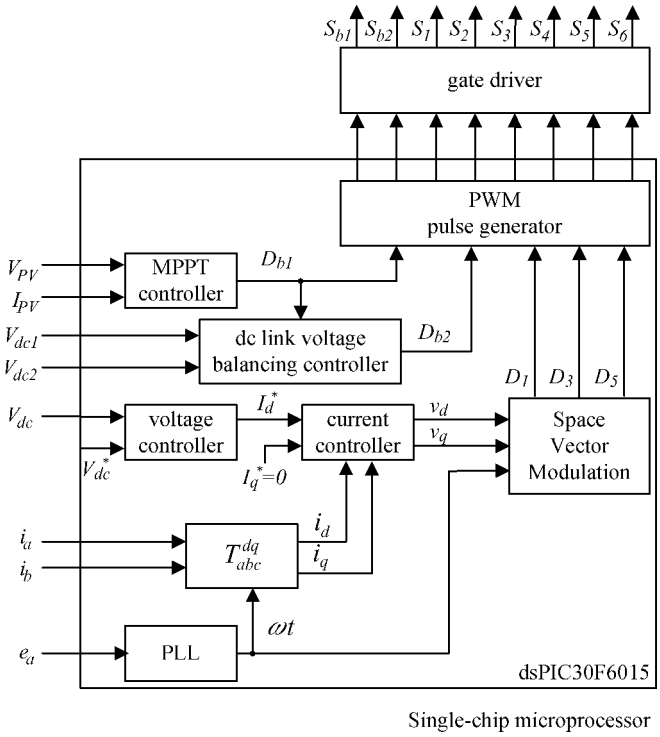

Fig. 8. Overall control diagram of the PV system.

TABLE I
PV ARRAY SPECIFICATIONS

PV array specifications	PV 1	PV 2
rated power	7 *kW*	10 *kW*
rated voltage	350 *V*	520 *V*
rated current	20 *A*	19.2 *A*
open-circuit voltage	380 *V*	620 *V*
short-circuit current	25 *A*	22 *A*

TABLE II
PV SYSTEM PARAMETERS

PV system parameters	value
grid voltage	3-phase 380 *V*, 60 *Hz*
switching frequency of switches	$f_s = 10$ *kHz*
input filter capacitor	$C_f = 10\,\mu F$
input filter inductor	$L_b = 2$ *mH*
dc link capacitor	C_{d1}, $C_{d2} = 4700\,\mu F$
output filter inductor	$L_o = 2$ *mH*
reference voltage of dc link	$V_{dc}^* = 620$ *V*

is minimized and the MPPT efficiency is increased. The variable power hysteresis P_h is adopted as

$$P_h = k_h P_{\mathrm{PV}} + P_{\mathrm{offset}} \tag{21}$$

where k_h and P_{offset} are a proportional factor and an offset power, respectively. The offset power P_{offset} is selected as a

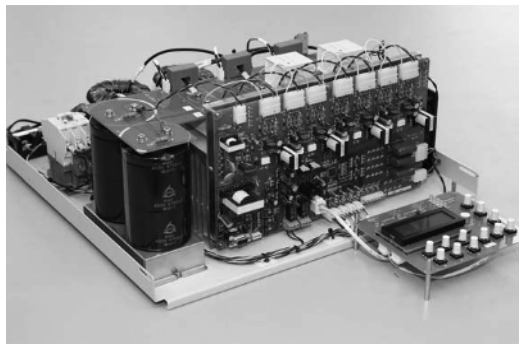

Fig. 9. Prototype of the proposed three-phase PV system.

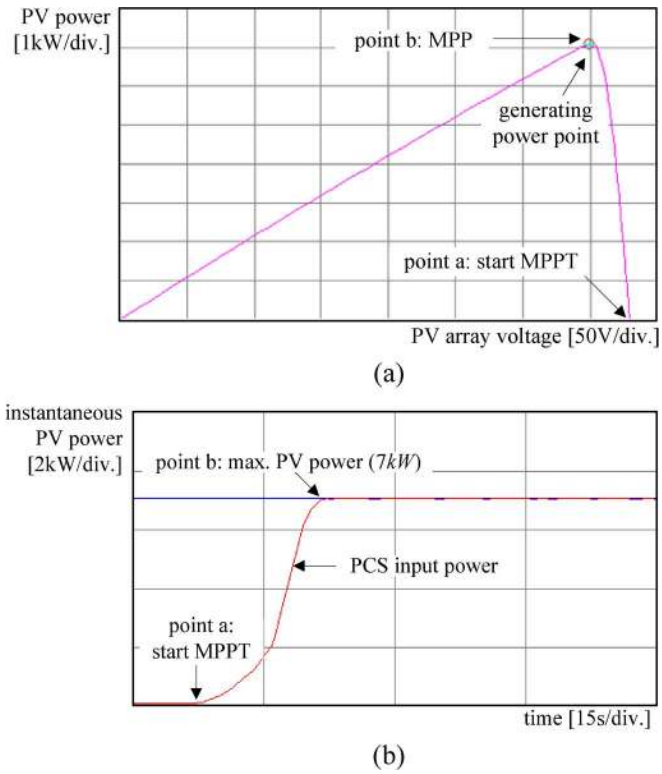

Fig. 10. Startup of the MPPT. (a) PV Power against PV voltage. (b) PV Power against time.

maximum measurement error 0.2% of the PV power system. To track the MPP, the constant value of k_h should be higher than the maximum peak-to-peak PV power variation at rated PV power. The selected value k_h was 0.01, which is the percent peak-to-peak PV power variation plus an additional 50% margin at rated PV power.

Fig. 10(a) and (b) show the startup behavior of the proposed MPPT control in a PV1 characteristic condition. Fig. 10(a) shows the PV power against PV voltage and (b) shows the PV power against time. The MPPT control is started at point a. After 15 s, the PCS input power reaches the maximum PV power at point b. The MPPT efficiency (MPPT effectiveness) is measured by Myway MWBFP APL2 simulator and MWBFP2-SIM simulation software. After the PCS input power reaches the MPP, the measured average PCS input power is

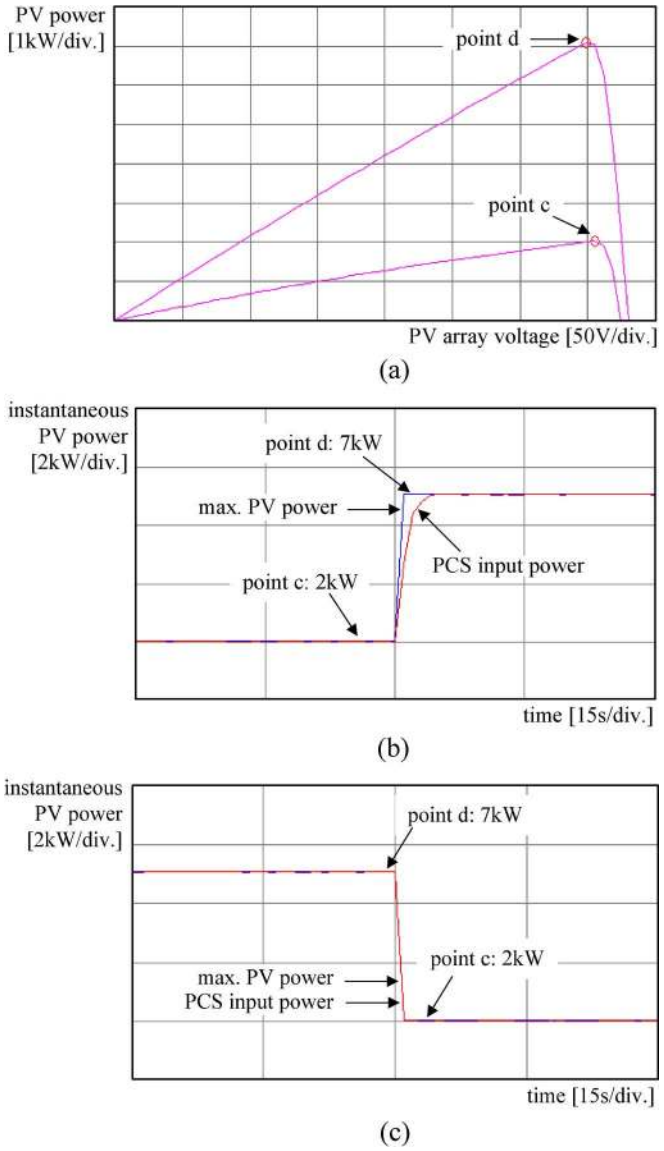

Fig. 11. Maximum PV array power and PCS input power. (a) PV array power of 2 (point c) and 7 kW (point d). (b) Maximum PV array power is changed abruptly from 2 to 7 kW (point c → point d). (c) Maximum PV array power is changed abruptly from 7 to 2 kW (point d → point c).

6.97 at 7 kW maximum PV power. The MPPT efficiency is obtained as

$$99.6\% = \frac{6.97\ \text{kW}}{7\ \text{kW}} \times 100\%. \tag{22}$$

Fig. 11(a)–(c) show the MPPT performance during abruptly transient PV power. When the maximum PV power is changed from 2 to 7 kW (point c → point d) during 1 s, the generating power is tracked to the new maximum PV power in about 3 s. When the maximum PV power is changed from 7 to 2 kW (point d → point c) during 1 s, the generating power is tracked to the new maximum power instantaneously.

Fig. 12(a) and (b) show the dc link voltage variation when the PV array power is changed abruptly. The dc link voltage variation is large when the conventional PI controller is adopted as shown in Fig. 12(a). However, the variation of the dc link voltage

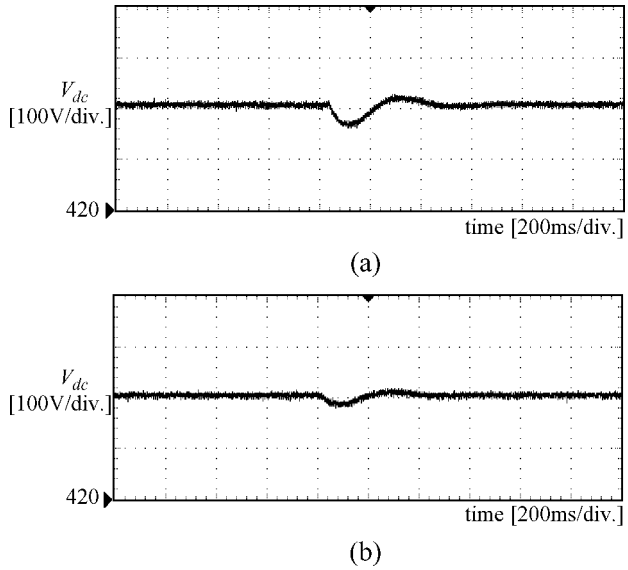

Fig. 12. DC link voltage of PV array power is changed suddenly. (a) DC link voltage when the weighted-error PI controller is not adopted. (b) DC link voltage when the weighted-error PI controller is adopted.

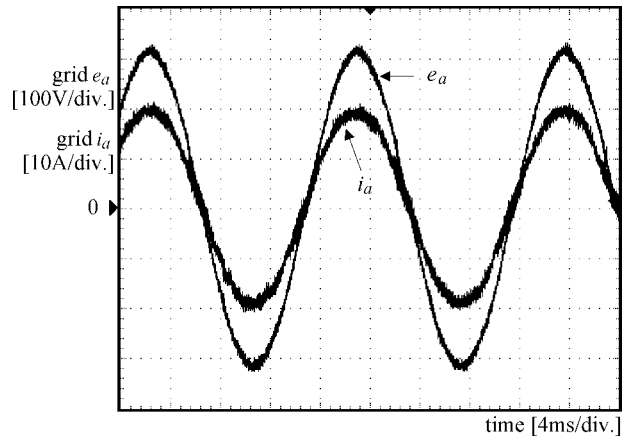

Fig. 13. Grid voltage and current waveforms.

is reduced when the weighted-error PI controller is adopted as shown in Fig. 12(b). This result shows the good performance of the weighted-error PI controller for fast dc link voltage control.

Fig. 13 shows the measured grid voltage and current waveforms at 10 kW. It explicitly shows that the grid current is sinusoidal and in phase with the grid voltage, which implies feeding only real power to the grid. The grid current produces a near-unity power factor of 99.5%, and its THD was measured at 2.0%. Additionally, each harmonic component was less than 1.1%. Thus, the THD and harmonic components were kept at low levels, and these also satisfy the following grid current regulation: THD less than 5% and each harmonic component less than 3%.

Fig. 14(a) shows the measured efficiency of the proposed PV system and a two-level boosting PV system which is composed of the conventional two-level boost converter and the three-phase inverter at full load. At the 300-V PV voltage where the reverse-recovery losses are significant, the power efficiency of the proposed system is 94%, a 2% increase in power efficiency. At the 600-V PV voltage where the reverse-recovery losses are not

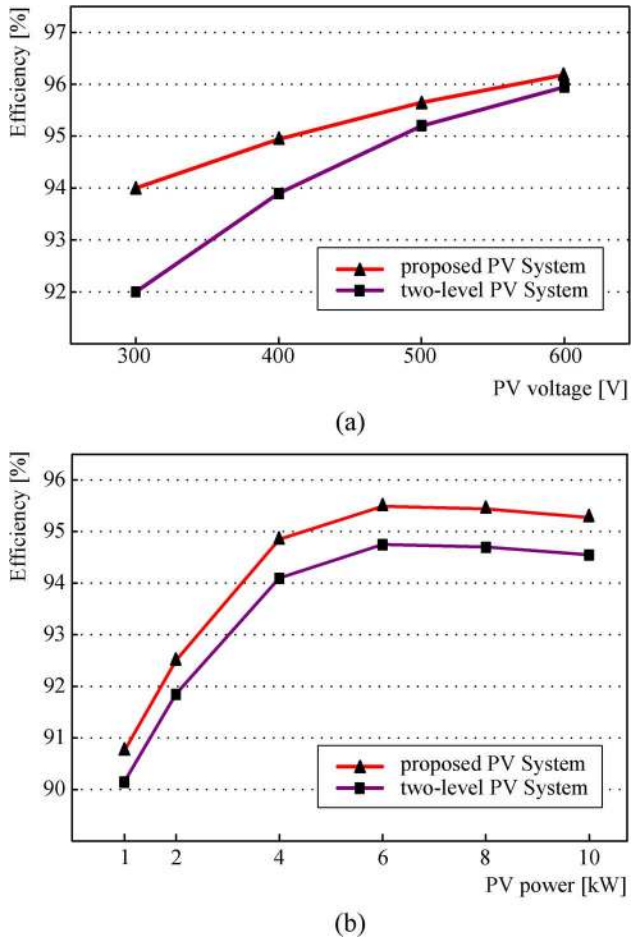

Fig. 14. Measured efficiency of the proposed PV system and the two-level PV system. (a) Against PV voltage at full load. (b) Against load at 450-V PV voltage.

severe, the power efficiency of the proposed system is 96.2%, a 0.2% increase in power efficiency. Fig. 14(b) shows the measured efficiency against the load at 450-V PV voltage, where the calculated European efficiency [20] is 94.1%. Compared with the conventional two-level boosting PV system, the power efficiency is increased 0.8%.

IV. Conclusion

A three-phase PV system with three-level boosting MPPT control is proposed. A simple MPPT control using a power hysteresis tracks the MPP, giving direct duty control for the three-level boost converter. The three-level boost converter reduces the reverse recovery losses of the diodes and increases the overall power efficiency. The weighted-error PI controller is suggested to control the dc link voltage faster. All algorithms and controllers are implemented on a single-chip microprocessor. Experimental results obtained on a 10-kW prototype show high performance of the proposed technique.

References

[1] T. Hiyama, S. Kouzuma, and T. Imakubo, "Identification of optimal operating point of PV modules using neural network for real time maximum power tracking control," *IEEE Trans. Energy Convers.*, vol. 10, no. 2, pp. 360–367, Jun. 1995.

[2] T. Hiyama and K. Kitabayashi, "Neural network based estimation of maximum power generation from PV module using environmental information," *IEEE Trans. Energy Convers.*, vol. 12, no. 3, pp. 241–247, Sep. 1997.

[3] J. H. Lee, H. S. Bae, and B. H. Cho, "Advanced incremental conductance MPPT algorithm with a variable step size," in *Proc. IEEE 12th Int. Power Electron. Motion Control Conf.*, Aug. 2006, pp. 603–607.

[4] J. M. Kwon, K. H. Nam, and B. H. Kwon, "Photovoltaic power conditioning system with line connection," *IEEE Trans. Ind. Electron.*, vol. 53, no. 4, pp. 1048–1054, Aug. 2006.

[5] W. Libo, Z. Zhengming, and L. Jianzheng, "A single-stage three-phase grid-connected photovoltaic system with modified MPPT method and reactive power compensation," *IEEE Trans. Energy Convers.*, vol. 22, no. 4, pp. 881–886, Dec. 2007.

[6] T. Esram and P. L. Chapman, "Comparison of photovoltaic array maximum power point tracking techniques," *IEEE Trans. Energy Convers.*, vol. 22, pp. 439–449, Jun. 2007.

[7] L. Egiziano, N. Femia, D. Granozio, and M. Vitelli, "Photovoltaic inverters with perturb & observe MPPT technique and one-cycle control," in *Proc. IEEE ISCAS*, 2006, pp. 3718–3721.

[8] N. Khaehintung, T. Wiangtong, and P. Sirisuk, "FPGA implementation of MPPT using variable step-size P&O algorithm for PV applications," in *Proc. IEEE ISCIT*, 2006, pp. 212–215.

[9] J. Enslin, M. Wolf, D. Snyman, and W. Sweigers, "Integrated photovoltaic maximum power point tracking converter," *IEEE Trans. Ind. Electron.*, vol. 44, pp. 769–773, Dec. 1997.

[10] Y. Huang, J. Wang, F. Z. Peng, and D. Yoo, "Survey of the power conditioning system for PV power generation," in *Proc. IEEE PESC*, Jun. 2006, pp. 1–6.

[11] R. Gonzalez, J. Lopez, P. Sanchis, and L. Marroyo, "Transformerless inverter for single-phase photovoltaic systems," *IEEE Trans. Power Electron.*, vol. 22, no. 2, pp. 693–697, Mar. 2007.

[12] E. Roman, R. Alonso, P. Ibanez, S. Elorduizapatarietxe, and D. Goitia, "Intelligent PV module for grid-connected PV systems," *IEEE Trans. Ind. Electron.*, vol. 53, no. 4, pp. 1066–1073, Aug. 2006.

[13] P. G. Barbosa, H. A. C. Braga, M. C. B. Rodrigues, and E. C. Teixeira, "Boost current multilevel inverter and its application on single-phase grid-connected photovoltaic systems," *IEEE Trans. Power Electron.*, vol. 21, no. 4, pp. 1116–1124, Jul. 2006.

[14] C. Liu and J. S. Lai, "Low frequency current ripple reduction technique with active control in a fuel cell power system with inverter load," *IEEE Trans. Power Electron.*, vol. 22, no. 4, pp. 1429–1436, Jul. 2007.

[15] I. S. Kim, M. B. Kim, and M. J. Youn, "New maximum power point tracker using sliding-mode observer for estimation of solar array current in the grid-connected photovoltaic system," *IEEE Trans. Ind. Electron.*, vol. 53, no. 4, pp. 1048–1054, Aug. 2006.

[16] M. T. Zhang, Y. Jiang, F. C. Lee, and M. M. Jovanovic, "Single-phase three-level boost power factor correction converter," in *Proc. IEEE APEC*, Mar. 1995, pp. 434–439.

[17] P. Barbosa, F. Canales, and F. Lee, "Analysis and evaluation of the two-switch three-level boost rectifier," in *Proc. IEEE PESC*, Jun. 2001, pp. 1659–1664.

[18] G. Yao, M. Ma, Y. Deng, W. Li, and X. He, "An improved ZVT PWM three level boost converter for power factor preregulator," in *Proc. IEEE PESC*, Jun. 2007, pp. 768–772.

[19] J. H. Youm and B. H. Kwon, "An effective software implementation of the space-vector modulation," *IEEE Trans. Ind. Electron.*, vol. 46, no. 4, pp. 866–868, Aug. 1999.

[20] H. Haberlin and L. Borgna, "Total efficiency—A new quantity for better characterization of grid connected PV inverters," presented at the 20th Euro. Photovoltaic Solar Energy Conf., Barcelona, Spain, 2005.

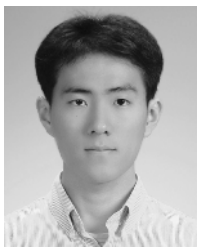

Jung-Min Kwon (S'08) was born in Ulsan, Korea, in 1981. He received the B.S. degree in electrical and electronic engineering from Yonsei University, Seoul, Korea, in 2004. He is currently pursuing the Ph.D. degree in electronic and electrical engineering from Pohang University of Science and Technology (POSTECH), Pohang, Korea.

His research interests include renewable energy, distributed generation, and switch-mode power supplies.

Bong-Hwan Kwon (M'91) was born in Pohang, Korea, in 1958. He received the B.S. degree from Kyungbuk National University, Taegu, Korea, in 1982, and the M.S. and Ph.D. degrees in electrical engineering from Korea Advanced Institute of Science and Technology, Seoul, Korea, in 1984 and 1987, respectively.

Since 1987, he has been with the Department of Electronic and Electrical Engineering, Pohang University of Science and Technology (POSTECH), Pohang, Korea, where he is currently a Professor. His research interests include renewable energy, high-frequency converters, and switch-mode power supplies.

Kwang-Hee Nam (S'83–M'86) was born in Seoul, Korea, in 1956. He received the B.S. and M.S. degrees in chemical technology and control and instrumentation engineering from Seoul National University, Seoul, Korea, in 1980 and 1982, respectively, and the M.S. and Ph.D. degrees in mathematics and electrical engineering from the University of Texas at Austin, Austin, in 1986.

He is currently a Professor with the Department of Electrical Engineering, Pohang University of Science and Technology (POSTECH), Pohang, Korea. His research interests include motor design and control, personnel rapid transit, computer networks, and nonlinear systems analysis.